Available online at www.sciencedirect.com
ScienceDirect
Journal of Sound and Vibration 312 (2008) 848–861
JOURNAL OF SOUND AND VIBRATION
www.elsevier.com/locate/jsvi

Adaptive vision-based control of a motor-toggle mechanism: Simulations and experiments

Chin-Wen Chuang[a], Ming-Shyan Huang[b], Kun-Yung Chen[b], Rong-Fong Fung[b,*]

[a]*Department of Electrical Engineering, I-Shou University, 1, Section 1, Hsueh-Cheng Road, Ta-Hsu Hsiang, Kaohsiung 840, Taiwan, ROC*
[b]*Department of Mechanical and Automation Engineering, National Kaohsiung First University of Science and Technology, 1 University Road, Yenchau, Kaohsiung 824, Taiwan, ROC*

Received 22 August 2007; received in revised form 22 August 2007; accepted 11 November 2007
Available online 21 December 2007

Abstract

The dynamic motion of an adaptive visual servoing feedback-controlled punching machine, which is made up by a toggle mechanism driven by a permanent magnet (PM) synchronous servomotor, is studied numerically and experimentally. First, Hamilton's principle, Lagrange multiplier, geometric constraints and partitioning method are employed to derive its dynamic equations for numerical simulations. To satisfy the demand of the machine performance, adaptive controller by using stability analysis with inertia-related Lyapunov function is designed to control the slider responses. Different from the previous studies, the vision servo system of a non-contact measurement of a charge-coupled device (CCD) camera is employed to measure the shape patterns as output states instead of using the expensive linear scale or encoder of the motor-mechanism system. Finally, the stable and robust control performances of an adaptive controller by the Lyapunov stable theory for a motor-toggle mechanism with external disturbances are proposed. A combination of the visual servoing measurement system and the motion control system are established experimentally for the motor-toggle mechanism system. From the agreements between numerical simulations and experimental results, it is demonstrated that the proposed controller, by use of machine vision, is robust to external disturbances for a punching machine system.

1. Introduction

The toggle mechanism has many applications where to overcome a large resistance with a small driving force is necessary, for example, clutches, rock crushers, truck tailgates, vacuum circuit breakers, pneumatic riveters, punching machines, forging machines, injection modeling machines, etc.

The motion controls of a toggle mechanism have been studied recently [1–6]. Lin et al. [1] proposed a fuzzy logic controller, which was based on the concept of hitting condition without using the complex mathematical model for a motor-mechanism system. The fuzzy neural network controller [2–4] was applied to control a motor-toggle servomechanism. The numerical results via the inverse dynamics control and variable structure control are compared [5] for an electrohydraulic actuated toggle mechanism. The variable structure control [6]

*Corresponding author. Tel./fax: +886 7 6011066.
E-mail address: rffung@ccms.nkfust.edu.tw (R.-F. Fung).

0022-460X/$ - see front matter © 2007 Elsevier Ltd. All rights reserved.
doi:10.1016/j.jsv.2007.11.019

was employed to a toggle mechanism, which was driven by a linear synchronous and the joint Coulomb friction was considered. In the adaptive control territory, Li et al. [7] proposed a hybrid control scheme for the flexible structures to obtain both good dynamic and static characteristics. A nonlinear strategy is proposed by Beji and Bestaoui [8] to ensure the vehicle control, in which the proof of main results is based on the Lyapunov concept. In these studies, the linear scale or encoder was employed as the sensor to feedback the position and speed.

In the previous papers [1–8], the controllers were difficult to realize if the feedback sensors could not be installed in the motor mechanisms for real operational conditions. Therefore, the non-contact measurement vision system exhibits its merit to measure the output state of the motor-mechanism systems. Petrovic and Brezak [9] applied the vision systems to motion control, in which the hard real-time constrains is placed on image processing and is suitable for real-time angle measurement. In the autonomous vehicle [10], the reference lane is continually detected by the machine vision system, and in order to cope with the steering delay and the side-slip of vehicle, the PI controller is employed for the yaw rate feedback. Park and Lee [11] presented the visual servoing control for a ball on a plate to track its desired trajectory by sliding mode control. Oscar and Ricardo [12] designed the adaptive controllers for the robot's positioning and tracking using direct visual feedback with camera-in-hand configurations. In the previous studies [9–12], they do not either discuss about the robustness of the vision system associated with the controllers or investigate robustness performances of the adaptive controllers for robot systems in experimental realization.

Adaptive control techniques are essential to provide a stable and robust performance for a wide range of applications, e.g. robot control, process control, etc., and most of the applications are inherently nonlinear. Moreover, relatively little general theories exist for the adaptive controls [13,14] of nonlinear systems. As the application of a motor-toggle mechanism has similar control problems to the robotic systems, the adaptive control technique developed by Slotine and Li [15,16], which exploited the conservation of energy formulation to design control laws for the fixed position control problem, is adopted to control the motor-toggle mechanism in this study. The techniques made use of matrix properties of a skew-symmetric system so that the measurements of acceleration signals and the computations of inverse of the inertia matrix are not necessary. Moreover, an inertia-related Lyapunov function containing a quadratic form of a linear combination of speed- and position-error states will be formulated.

In this paper, the machine vision system is used as the sensor to measure the output state of the punching machine in real operational conditions. The main advantage of a vision-based measuring system is its non-contact measurement principle, which is important in cases when the contact measurements are difficult to implement. In the theoretical analysis, Hamilton's principle, Lagrange multiplier, geometric constraints and the partitioning method are employed to derive the dynamic equations. Main contribution of this paper is that the adaptive vision-based controller is proposed to compare the performances with external disturbances numerically and experimentally.

2. Dynamic analysis of a motor-toggle mechanism

2.1. Mathematical model of the motor-toggle mechanism

The toggle mechanism driven by a PM synchronous servomotor is shown in Fig. 1(a) and its experimental equipment is shown in Fig. 1(b). The screw is a media that makes the small torque τ to convert into the large force F_C acting on the slider C. The conversion relationship is

$$\tau = \frac{F_C l_d}{2\pi n}, \tag{1}$$

where l_d is the lead of screw and n is the gear ratio number. Comparing with the previous studies [1,5,6], it is seen that the new toggle mechanism has the special designs of r_1 and r_2 being in the same link and having a right triangle, and the lengths of links 1 and 3 are the same, i.e., $r_1 = r_3$. Therefore, the relation between slider B and angle θ_1 can be found as follows: $x_B = 2r_1 \cos\theta_1$.

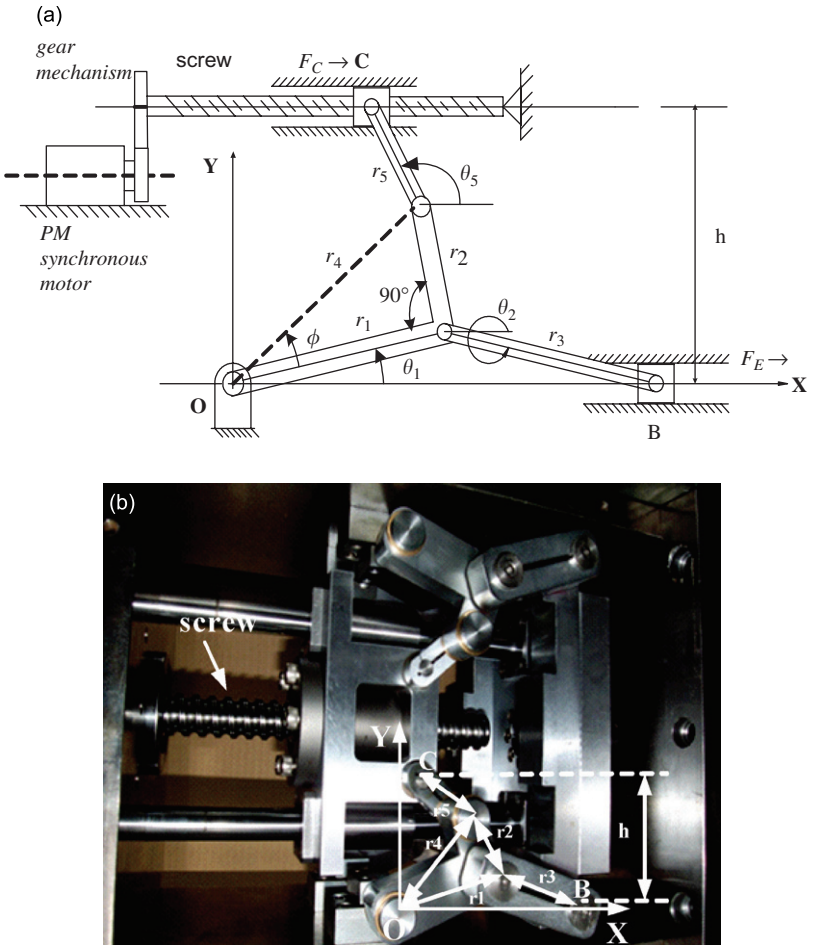

Fig. 1. The toggle mechanism driven by a PM synchronous servo motor. (a) The physical model. (b) The experimental equipment.

Fung et al. [5,6] have exploited the holomonic constraint equation as follows:

$$\mathbf{\Phi}(\boldsymbol{\theta}) = \begin{bmatrix} r_3 \sin\theta_2 + r_1 \sin\theta_1 \\ r_5 \sin(\pi - \theta_5) + r_4 \sin(\theta_2 + \phi) - h \end{bmatrix} = 0, \tag{2}$$

where $\boldsymbol{\theta} = [\theta_5 \ \theta_2 \ \theta_1]^{\mathrm{T}}$ is the vector of generalized coordinates. Similar to the previous studies [1,5,6], one obtains the Euler–Lagrange equation of motion, accounting for both the applied and constraint forces, as

$$\mathbf{M}(\boldsymbol{\theta})\ddot{\boldsymbol{\theta}} + \mathbf{N}(\boldsymbol{\theta}, \dot{\boldsymbol{\theta}}) - \mathbf{B}\mathbf{U} - \mathbf{D} + \mathbf{\Phi}_{\theta}^{\mathrm{T}}\lambda = 0, \tag{3}$$

and the details of **M**, **N**, **B**, **U** and **D** can also be found in Fung et al. [5,6]. Taking the first and second derivatives of the constraint position equation (2):

$$\mathbf{\Phi}_{\theta}\dot{\boldsymbol{\theta}} = \begin{bmatrix} r_3\dot{\theta}_2 \cos\theta_2 + r_1\dot{\theta}_1 \cos\theta_1 \\ r_5\dot{\theta}_5 \cos\theta_5 + r_4\dot{\theta}_1 \cos(\theta_1 + \phi) \end{bmatrix} = 0, \tag{4}$$

$$\mathbf{\Phi}_{\theta}\ddot{\boldsymbol{\theta}} = -(\mathbf{\Phi}_{\theta}\dot{\boldsymbol{\theta}})_{\theta}\dot{\boldsymbol{\theta}} = \gamma = \begin{bmatrix} r_3\dot{\theta}_2^2 \sin\theta_2 + r_1\dot{\theta}_1^2 \sin\theta_1 \\ r_5\dot{\theta}_5^2 \sin\theta_5 + r_4\dot{\theta}_1^2 \sin(\theta_1 + \phi) \end{bmatrix} = 0. \tag{5}$$

Using these equations and Euler Lagrange equation (3), we obtain the equation in the matrix form as

$$\begin{bmatrix} \mathbf{M} & \mathbf{\Phi}_\theta^{\mathrm{T}} \\ \mathbf{\Phi}_\theta & 0 \end{bmatrix} \begin{bmatrix} \ddot{\boldsymbol{\theta}} \\ \lambda \end{bmatrix} = \begin{bmatrix} \mathbf{B}\mathrm{U} + \mathbf{D}(\boldsymbol{\theta}) - \mathbf{N}(\boldsymbol{\theta}, \dot{\boldsymbol{\theta}}) \\ \gamma \end{bmatrix}. \tag{6}$$

This is a system of differential–algebraic equations.

2.2. Reduced formulation of the differential equations of motion

The motion equations of the toggle mechanism are summarized in the matrix form of Eq. (6) and the constraint equation (2). The following implicit method is employed to reduce the system equations.

Equations (2) and (6) may be reordered and partitioned according to the decomposition of $\boldsymbol{\theta} = [\theta_5 \ \ \theta_2 \ \ \theta_1]^{\mathrm{T}} = [\mathbf{u}^{\mathrm{T}} v^{\mathrm{T}}]^{\mathrm{T}}$ which is the same as Ref. [1]. Thus, Eqs. (6) and (7) can be written in the matrix form as

$$\hat{M}(v)\ddot{v} + \hat{N}(v, \dot{v}) = \hat{Q}U + \hat{D}, \tag{7}$$

where

$$\hat{M} = M^{vv} - \mathbf{M}^{vu}\mathbf{\Phi}_u^{-1}\mathbf{\Phi}_v - \mathbf{\Phi}_v^{\mathrm{T}}\left(\mathbf{\Phi}_u^{-\mathbf{1}}\right)^{\mathbf{T}}\left[\mathbf{M}^{uv} - \mathbf{M}^{uu}\mathbf{\Phi}_u^{-\mathbf{1}}\mathbf{\Phi}_v\right],$$
$$\hat{N} = \left[N^v - \mathbf{\Phi}_v^{\mathrm{T}}\left(\mathbf{\Phi}_u^{-\mathbf{1}}\right)^{\mathbf{T}}\mathbf{N}^u\right] + \left[\mathbf{M}^{vu}\mathbf{\Phi}_u^{-\mathbf{1}} - \mathbf{\Phi}_v^{\mathrm{T}}\left(\mathbf{\Phi}_u^{-\mathbf{1}}\right)^{\mathbf{T}}\mathbf{M}^{uu}\mathbf{\Phi}_u^{-1}\right]\gamma,$$
$$\hat{Q} = B^v - \mathbf{\Phi}_v^{\mathrm{T}}\left(\mathbf{\Phi}_u^{-1}\right)^{\mathrm{T}}\mathbf{B}^u, \quad U = \left[i_q^*\right], \quad \hat{D} = D^v - \mathbf{\Phi}_v^{\mathrm{T}}\left(\mathbf{\Phi}_u^{-1}\right)^{\mathrm{T}}\mathbf{D}^u.$$

The elements of the vectors $\mathbf{u}$, $\mathbf{v}$ and matrices $\mathbf{\Phi}_u$, $\mathbf{\Phi}_v$, $\mathbf{M}^{uu}$, $\mathbf{M}^{uv}$, $\mathbf{M}^{vu}$, M^{vv}, $\mathbf{N}^u$ and N^v are detailed in Ref. [1]. The resultant equation (7) is a differential equation with only one independent generalized coordinate v, which is the rotation angle θ_1 of link 1 in Fig. 1(a). The system becomes an initial value problem and can be integrated by using the fourth-order Runge–Kutta method.

2.3. Field-oriented PM synchronous motor drive

A machine model [17] of a PM synchronous motor can be described in a rotating rotor and the electric torque equation for the motor dynamics is

$$\tau_e = \tau_m + B_m\omega_r + J_m\dot{\omega}_r, \tag{8}$$

where τ_m is the load torque, B_m is the damping coefficient, ω_r is the rotor speed and J_m is the moment of inertia.

With the implementation of field-oriented control, the PM synchronous motor drive system can be simplified to a control system block diagram as shown in Fig. 2, in which

$$\tau_e = K_t i_q^*, \tag{9}$$

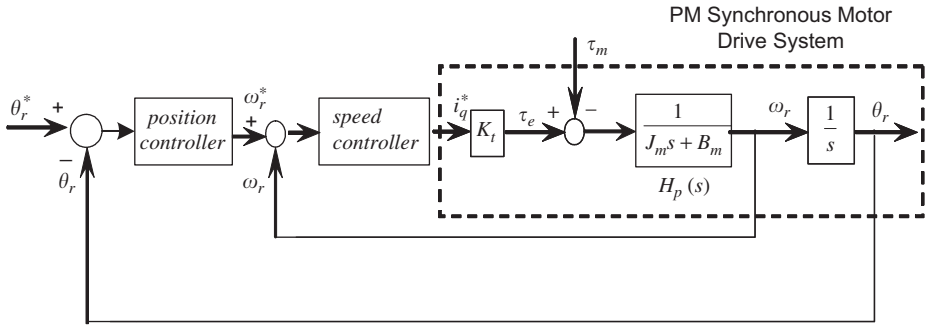

Fig. 2. A simplified control block diagram.

$$K_t = \tfrac{3}{2} P L_{md} I_{fd}, \tag{10}$$

$$H_p(s) = \frac{1}{J_m s + B_m}, \tag{11}$$

where i_q^* is the torque current command. By substituting Eq. (9) into Eq. (8), the applied torque can be obtained as follows:

$$\tau_m = K_t i_q - J_m \dot{\omega}_r - B_m \omega_r, \tag{12}$$

where τ_m is the torque applied in the direction of ω_r, and the variables ω_r and $\dot{\omega}_r$ are the angular speed and acceleration of the rotor, respectively.

3. Design of an adaptive vision-based controller

The adaptive vision-based control system is shown in Fig. 3, where x_B^*, x_B and θ_1 are the slider command position, slider position and the rotation angle of link 1 of the motor-mechanism system, respectively. The slider position x_B is the desired control objective and can be manipulated by the relation $x_B = 2r_1 \cos\theta_1$, where angle θ_1 is the experimental measured state using a shape pattern in the machine vision system.

In order to design an adaptive control, we rewrite Eq. (7) as the second-order nonlinear one:

$$U(t) = f(\mathbf{X};\ t)\ddot{v}(t) + G(\mathbf{X};\ t) - d(t), \tag{13}$$

where

$$f(\mathbf{X};\ t) = \hat{Q}^{-1}\hat{M},\quad G(\mathbf{X};\ t) = \hat{Q}^{-1}\hat{N},\quad d(t) = \hat{Q}^{-1}\hat{D},$$

and $U(t)$ is the control input current i_q^*. It is assumed that the mass of slider B and the external force F_E are not exactly known. With these uncertainties, the first step in designing an adaptive vision-based controller is to select a Lyapunov function, which is a function of tracking error and the parameters' errors. An inertia-related Lyapunov function [15,16,18] containing a quadratic form of a linear combination of speed- and position-error states is chosen as follows:

$$V = \tfrac{1}{2} s^{\mathrm{T}} f(X;\ t) s + \tfrac{1}{2}\tilde{\varphi}^{\mathrm{T}}\Gamma^{-1}\tilde{\varphi}, \tag{14}$$

where

$$s = \lambda_e e + \dot{e},\quad e = x_B - x_B^*,\quad \Gamma = \begin{bmatrix} \gamma_1 & 0 \\ 0 & \gamma_2 \end{bmatrix},$$

$$\tilde{\varphi} = \varphi - \hat{\varphi},\quad \varphi = \begin{bmatrix} m_B \\ F_E \end{bmatrix},\quad \hat{\varphi} = \begin{bmatrix} \hat{m}_B \\ \hat{F}_E \end{bmatrix},$$

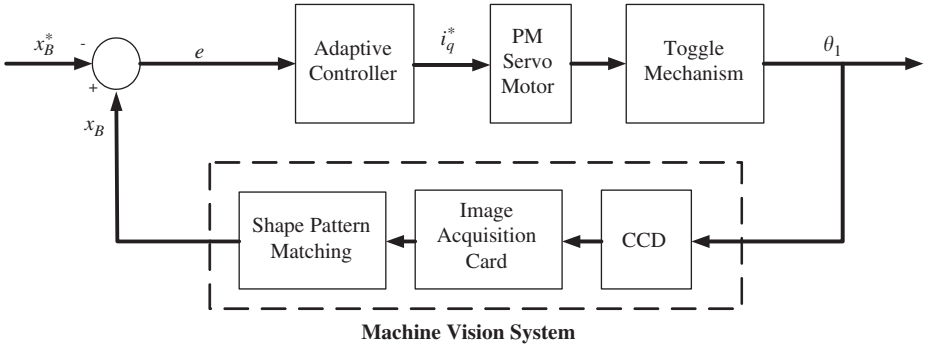

Fig. 3. Block diagram of an adaptive vision-based control system.

and λ_e, γ_1 and γ_2 are positive scalar constants. The auxiliary signal s may be considered as a filtered tracking error.

Differentiating Eq. (14) with respect to time gives

$$\dot{V} = s^{\mathrm{T}} f(X;\ t)\dot{s} + \tfrac{1}{2} s^{\mathrm{T}} \dot{\hat{Q}}^{-1} \hat{M} s + \tfrac{1}{2} s^{\mathrm{T}} \hat{Q}^{-1} \dot{\hat{M}} s + \tilde{\varphi}^{\mathrm{T}} \Gamma^{-1} \dot{\tilde{\varphi}} \tag{15}$$

and multiplying the variable $\dot{s}$ with Eq. (13), we have

$$\begin{aligned} f(X;\ t)\dot{s} &= f(X;\ t)(\lambda_e \dot{e} - \ddot{x}_B^* + \ddot{x}_B) \\ &= f(X;\ t)(\lambda_e \dot{e} - \ddot{x}_B^*) + f(X;t)\ddot{x}_B \\ &= Y(\bullet) + Z(\bullet)\varphi - 2r_1 \sin\theta_1 U, \end{aligned} \tag{16}$$

where $Y(\bullet)$ and $Z(\bullet)$ can be found in Appendix A. Substituting Eq. (16) into Eq. (15) gives

$$\begin{aligned} \dot{V} &= s^{\mathrm{T}}(Y(\bullet) + Z(\bullet)\varphi - 2r_1 \sin\theta_1 U) + \tfrac{1}{2} s^{\mathrm{T}} \dot{\hat{Q}}^{-1} \hat{M} s + \tfrac{1}{2} s^{\mathrm{T}} \hat{Q}^{-1} \dot{\hat{M}} s + \tilde{\varphi}^{\mathrm{T}} \Gamma^{-1} \dot{\tilde{\varphi}} \\ &\equiv s^{\mathrm{T}}(Y'(\bullet) + Z'(\bullet)\varphi - 2r_1 \sin\theta_1 U) + \tilde{\varphi}^{\mathrm{T}} \Gamma^{-1} \dot{\tilde{\varphi}}, \end{aligned} \tag{17}$$

where $Y'(\bullet)$ and $Z'(\bullet)$ can also be found in Appendix A. If the control input is selected as

$$U = \frac{1}{2r_1 \sin\theta_1}(Y'(\bullet) + Z'(\bullet)\hat{\varphi} + K_V s), \tag{18}$$

where K_V is a positive constant. Eq. (17) becomes

$$\dot{V} = -s^{\mathrm{T}} K_V s + \tilde{\varphi}^{\mathrm{T}}(\Gamma^{-1} \dot{\tilde{\varphi}} + Z'(\bullet)^{\mathrm{T}} s). \tag{19}$$

By selecting the adaptive update rule as

$$\dot{\tilde{\varphi}} = -\dot{\hat{\varphi}} = -\Gamma Z'(\bullet)^{\mathrm{T}} s, \tag{20}$$

and substituting into Eq. (19), it then becomes

$$\dot{V} = -s^{\mathrm{T}} K_V s \leqslant 0. \tag{21}$$

As $\dot{V}$ in Eq. (21) is negative semi-definite, then V in Eq. (14) is upper-bounded. As V is upper-bounded and $f(\mathbf{X}; t)$ is a positive-definite matrix, it can be said that s and $\tilde{\varphi}$ are bounded. Let function $P(t) = -\dot{V}(t) = s^{\mathrm{T}} K_V s$, and integrate function $P(t)$ with respect to time

$$\int_0^t P(t)\,\mathrm{d}t = V(0) - V(t). \tag{22}$$

Because $V(0)$ is bound, and $V(t)$ is non-increasing and bounded, therefore

$$\lim_{t\to\infty} \int_0^t P(\tau)\,\mathrm{d}\tau < \infty. \tag{23}$$

Differentiate $P(t)$ with respect to time

$$\dot{P}(t) = s^{\mathrm{T}} K_V \dot{s} + \dot{s}^{\mathrm{T}} K_V s. \tag{24}$$

Since K_V, s, and $\dot{s}$ are bounded, $P(t)$ is uniformly continuous. From the above description, Barbalat's Lemma [19] can be used to state that

$$\lim_{t\to\infty} P(t) = 0. \tag{25}$$

Therefore, the following can be obtained:

$$\lim_{t\to\infty} s = 0. \tag{26}$$

As a result, the system is asymptotically stable. Moreover, the tracking error of the system will converge to zero according to $s = \lambda_e e + \dot{e}$ [15].

4. Numerical simulations

For numerical simulations, the external disturbance force F_E will be added to test the robustness of the adaptive controller, and the parameters of the motor-toggle mechanism are chosen as follows:

$$m_B = 4.12\,\text{kg}, \quad m_C = 5.58\,\text{kg}, \quad m_2 = 1.82\,\text{kg}, \quad m_3 = 1.61\,\text{kg},$$
$$m_5 = 0.95\,\text{kg}, \quad \mu = 0.17 \quad r_1 = 0.06\,\text{m}, \quad r_2 = 0.032\,\text{m}, \quad r_3 = 0.06\,\text{m}, \quad r_4 = 0.068\,\text{m},$$
$$r_5 = 0.03\,\text{m}, \quad h = 0.068\,\text{m}, \quad \phi = 0.4899\,\text{rad}, \quad K_t = 0.5652\,\text{N m/A},$$
$$J_m = 6.7 \times 10^{-5}\,\text{N m s}^2, \quad \text{and} \quad B_m = 1.12 \times 10^{-2}\,\text{N m s/rad}.$$

By substituting the above known parameters into Eq. (9), the system becomes an initial value problem and can be integrated using the fourth-order Runge–Kutta method with time step $\Delta t = 0.001$ s and tolerance error 10^{-9}. In the numerical simulations, the control objective is to control the position of slider B to move from the left- to the right-side end. The initial position of $x_B(0)$ is 0.06 m, the desired position x_B^* is 0.1 m and the controlled stroke of slider B, Δx_B, is equal to 0.04 m.

The gains of the adaptive control law (25) are given as follows:

$$\lambda_e = 10, \quad K_V = 194, \quad \gamma_1 = 248, \quad \text{and} \quad \gamma_2 = 173.$$

They are chosen to achieve the best transient performance in the limitation of control effort and the requirement of stability. In a real system, the angles of θ_1, θ_2, and θ_5 are limited in the following range: $23^\circ < \theta_1 < 63^\circ$, $325^\circ < \theta_2 < 350^\circ$, and $145^\circ < \theta_5 < 170^\circ$. Therefore, the invertible property of $\hat{Q}$ can be guaranteed and the system function $f(\mathbf{X}; t) = \hat{Q}^{-1}\hat{M} > 0$ can be proved.

The dynamic responses of slider B and the control efforts i_q^* with and without external disturbance force are compared in Figs. 4(a) and (b), respectively. The dotted lines are the desired positions, the dash lines are the transient responses of numerical simulations with external disturbance force $F_E = 0$ N and the solid lines are for $F_E = -100$ N. The negative sign in the external disturbance force indicates that the action direction is opposite to the X-direction in Fig. 1(a). In Fig. 4(a), the transient responses are almost the same and are stable after 0.5 s and the steady-state error is about 1×10^{-5} m. Since the transient responses are almost the same in the presence of uncertainties, it shows that the proposed adaptive control is robust. In Fig. 4(b), the maximum control effort $i_q^* = 0.218$ A for $F_E = 0$ N is smaller than $i_q^* = 0.710$ A for $F_E = -100$ N.

5. Experiments

In real operations of an experimental system, the main merit of this study is that the machine vision system of a digital CCD camera is employed as an unconstrained feedback sensor. In Fig. 5, the state angle θ_1 of the motor-toggle mechanism system is difficult to be measured by an installed encoder and thus is experimentally measured by a shape pattern of the machine vision system, which is needed only to paste a pattern on where one wants it to be measured and can be controlled to the desired position by a digital CCD camera.

5.1. Visual control system

The machine vision servoing system used in this paper takes a shape pattern pasted on the link and is shown in Fig. 5. It has the advantage of differentiating the link from its near monotonic surrounding fast and the directional shape pattern is easily identified by measuring the angle θ_1 of the motor-mechanism system. In this vision system, one full-frame of image consists of 752×582 pixels. Searching the whole video data of a full-frame for the shape pattern usually takes a long time, and degrades the performance of the visual servoing system. Thus, based on the range of angle θ_1, the image frame is adjusted by a CCD camera to contain the controlled degree of angle θ_1.

Pattern matching is the first step in implementing the machine vision system. Its servoing control algorithm is implemented by LabVIEW and the image acquisition card is implemented by PCI 1405. In the controlled image frame, the shape pattern is selected as the region of interest (ROI) to save in a disk for searching. Finally, the shape pattern matching algorithm is realized by LabVIEW and the position of slider B is

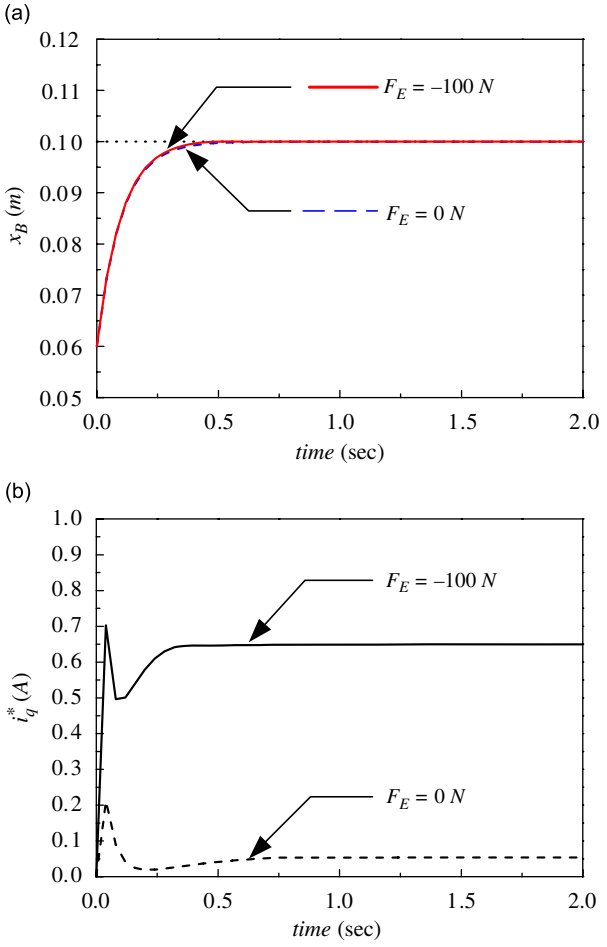

Fig. 4. The numerical simulations of a motor-toggle mechanism by an adaptive controller with and without external disturbance forces are compared: (a) the dynamic responses of slider B and (b) the control efforts i_q^*.

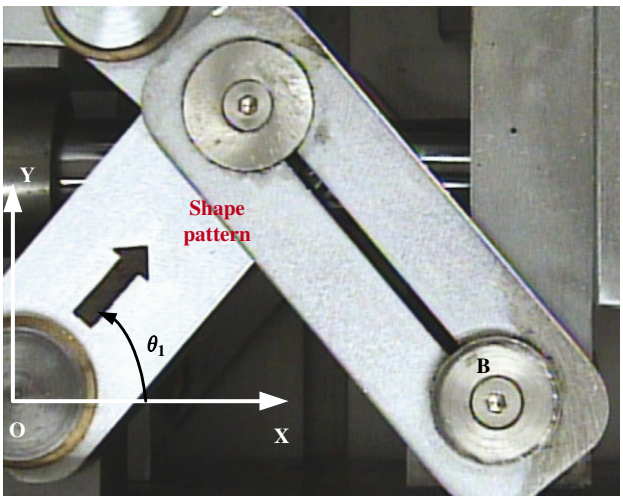

Fig. 5. The control image frame with a shape pattern.

controlled by the adaptive visual controller. In this paper, the image processing time is 0.2 s using the CCD camera to feedback the slider position.

5.2. Experimental setup

The visual control block diagram of the motor-toggle mechanism is shown in Fig. 6(a) and its experimental instruments are shown in Fig. 6(b). The control algorithm is implemented by using a Pentium computer and the control software is LabVIEW. The PM synchronous servomotor is implemented by the MITSUBISHI HC-KFS43 series. The specifications are described as follows: rated output 400 W, rated torque 1.3 N m, rated rotation speed 3000 rev/min and rated current 2.3 A. The servo is implemented by the MITSUBISHI

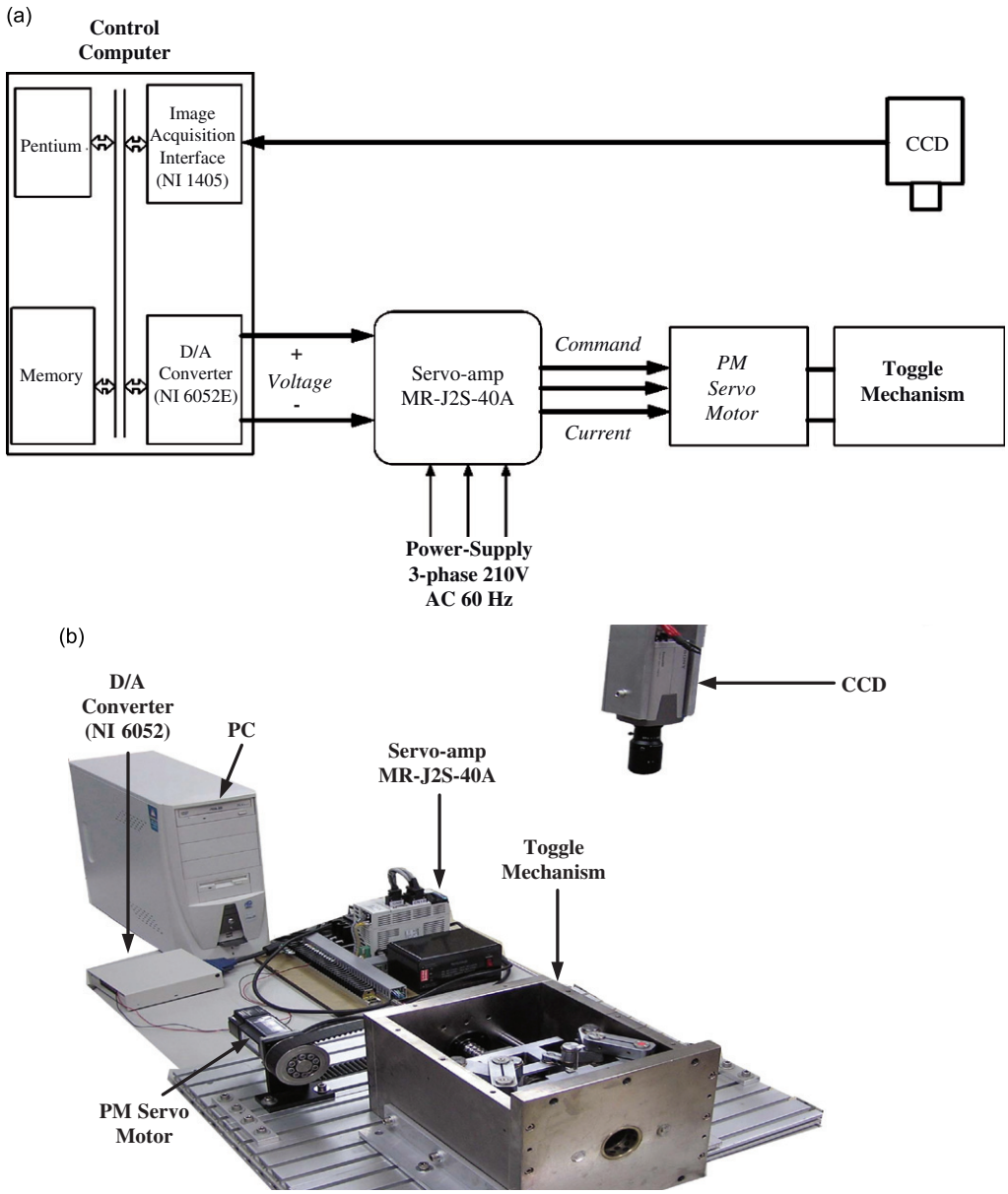

Fig. 6. The visual control system of a motor-toggle mechanism: (a) the computer control block diagram and (b) the experimental equipments.

MR-J2S-40A1. The control system is a sine-wave PWM control, which is a current control system. The digital CCD camera is implemented by the SONY SSC-DC393 series. The specifications are described as follows: imaging device 1/3-type interline transfer, picture elements 752(horizontal) × 582(vertical), and Lent CS-mount.

5.3. Experimental results

The initial state is $x_B(0) = 0.06\,\text{m}$ and the desired position is $x_B^* = 0.1\,\text{m}$. The adaptive vision-based control for the motor-mechanism system is performed by comparing the external disturbance force $F_E = 0\,\text{N}$ with $F_E = -10\,\text{N}$. The experimental results of the measured angle θ_1 via the machine vision system, the transient responses of slider B via the manipulating relation $x_B = 2r_1 \cos\theta_1$ and the control efforts i_q^* are shown in Figs. 7–9, respectively. It is seen that the experimentally measured angle θ_1 in Fig. 7 and the transient responses of slider B in Fig. 8 are almost the same for the system with and without F_E, and are stable after 0.75 s. However, the control efforts i_q^* are quite different. The maximum control effort $i_q^* = 0.28\,\text{A}$ for $F_E = 0\,\text{N}$ is smaller than $i_q^* = 0.75\,\text{A}$ for $F_E = -10\,\text{N}$. The maximum control efforts are near to those of numerical simulations.

Moreover, in order to demonstrate the robust control performance of the adaptive vision-based controller, the experiments are performed by suddenly adding an extra mass of 10 kg on slider B at 0.6 s, and suddenly adding 10 N on the external force at 0.6 s. Fig. 10 shows the good performance of regulation problems, and Fig. 11 shows the control input efforts, where the jumps occur when the extra mass and external force are suddenly added.

6. Conclusions

This paper successfully demonstrates the application of the proposed adaptive vision-based controller to position control the punching machine, which is made up by the toggle mechanism driven by a field-oriented PM synchronous servomotor. In order to overcome the general difficulties of non-contact measuring and external force uncertainties of the motor-mechanism system, a shape pattern is designed to measure the rotating angle and the adaptive visual servo controller is adopted. Finally, the numerical simulations and experimental results are provided to demonstrate the robust control performance of the proposed adaptive vision-based control. It is concluded that the main contributions of this study are to combine the visual servoing measurement system with the motion control system for the motor-toggle mechanism system and to demonstrate the stable and robust control performances of an adaptive controller by the Lyapunov stable theory with external disturbances.

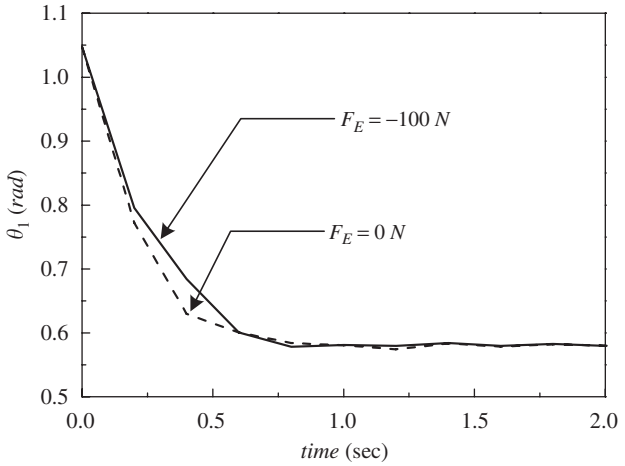

Fig. 7. The experimental measured angle θ_1 with and without external disturbance forces.

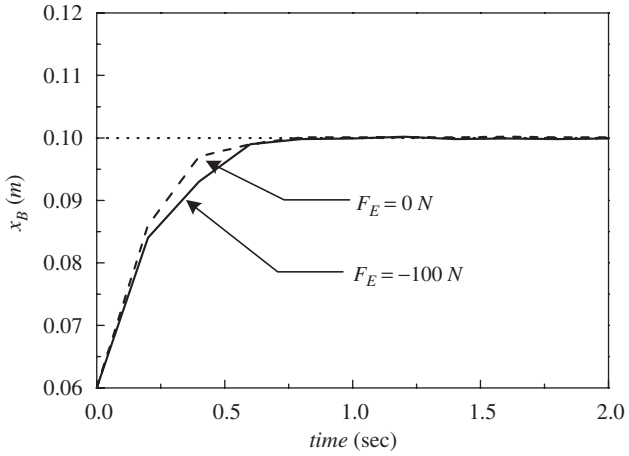

Fig. 8. The experimental dynamic responses of slider B with and without external disturbance forces.

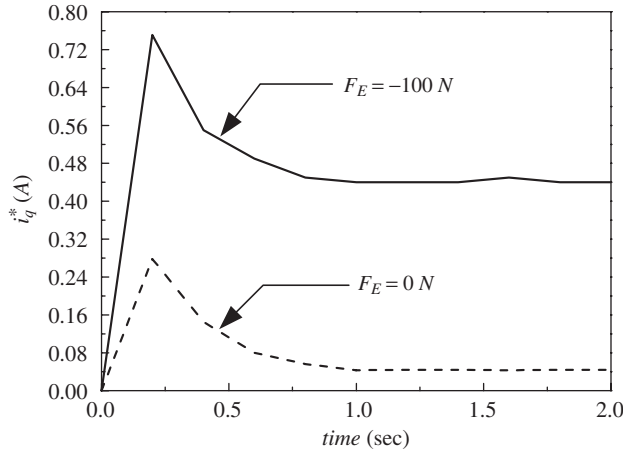

Fig. 9. The experimental control efforts i_q^* of a motor-toggle mechanism with and without external disturbance forces.

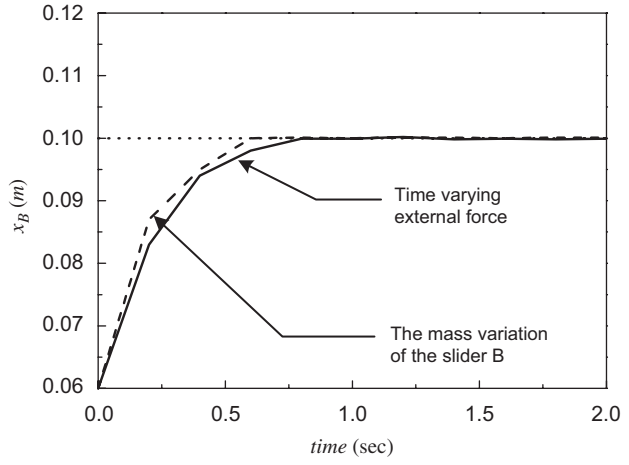

Fig. 10. The experimental dynamic responses of slider B with time-varying external force and mass variation at slider B.

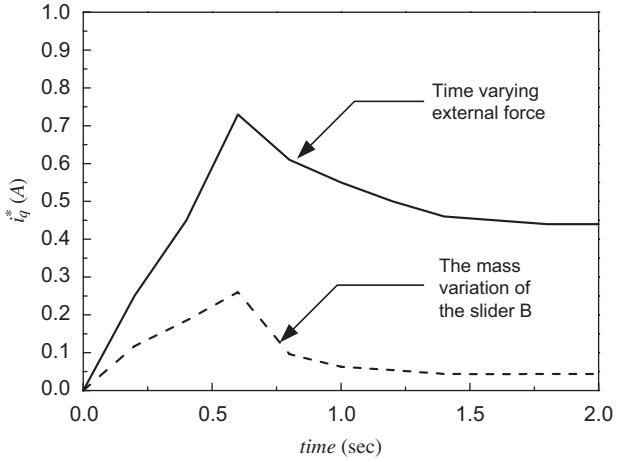

Fig. 11. The experimental control efforts i_q^* of a motor-toggle mechanism with time-varying external force and mass variation at slider B.

Acknowledgment

Support of this work by the National Science Council of the Republic of China Contract NSC-93-2745-E-327-001 is gratefully acknowledged.

Appendix A. Adaptive controller formulation

According to Eq. (9), the parameters can be separated as follows:

$$\begin{aligned}\hat{M} &= M^{vv} - \mathbf{M}^{vu}\boldsymbol{\Phi}_u^{-1}\boldsymbol{\Phi}_v - \boldsymbol{\Phi}_v^{\mathrm{T}}(\boldsymbol{\Phi}_u^{-1})^{\mathrm{T}}[\mathbf{M}^{uv} - \mathbf{M}^{uu}\boldsymbol{\Phi}_u^{-1}\boldsymbol{\Phi}_v]\\ &= -\frac{1}{3}m_3r_1^2 - \frac{1}{3}m_5r_4^2\cos^2(\phi+\theta_1)\sec^2\theta_5 - \frac{1}{2r_2^2}m_2r_1^2r_4^2\sin^2\phi\\ &\quad - 2m_3r_1^2\sin^2\theta_1 - (m_5r_4^2 + m_Cr_4^2 + J_mr_4^2Z^2)\sin^2(\phi+\theta_1)\\ &\quad + (m_5r_4^2 + 2m_Cr_4^2 + 2J_mr_4^2Z^2)\cos(\phi+\theta_1)\sin(\phi+\theta_1)\tan\theta_5\\ &\quad - (m_Cr_4^2 + J_mr_4^2Z^2)\cos^2(\phi+\theta_1)\tan^2\theta_5 + m_B(-4r_1^2\sin^2\theta_1)\\ &\equiv \hat{M}_1 + m_B\hat{M}_2,\end{aligned} \tag{A.1}$$

$$\begin{aligned}\hat{N} &= [N^v - \boldsymbol{\Phi}_v^{\mathrm{T}}(\boldsymbol{\Phi}_u^{-1})^{\mathrm{T}}\mathbf{N}^u] + [\mathbf{M}^{vu}\boldsymbol{\Phi}_u^{-1} - \boldsymbol{\Phi}_v^{\mathrm{T}}(\boldsymbol{\Phi}_u^{-1})^{\mathrm{T}}\mathbf{M}^{uu}\boldsymbol{\Phi}_u^{-1}]\gamma\\ &= -B_mr_4^2Z^2\sin^2(\phi+\theta_1)\dot{\theta}_1 - 2m_3r_1^2\cos\theta_1\sin\theta_1\dot{\theta}_1^2\\ &\quad - (m_5r_4^2 + m_Cr_4^2)\cos(\phi+\theta_1)\sin(\phi+\theta_1)\dot{\theta}_1^2 - J_mr_4^2Z^2\cos(\phi+\theta_1)\sin(\phi+\theta_1)\dot{\theta}_1^2\\ &\quad + \tfrac{1}{3}m_5r_4^2\cos(\phi+\theta_1)\sec^2\theta_5\sin(\phi+\theta_1)\dot{\theta}_1^2 - B_mr_4r_5Z^2\sin(\phi+\theta_1)\sin\theta_5\dot{\theta}_5\\ &\quad - (\tfrac{1}{2}m_5r_4r_5 + m_Cr_4r_5 + J_mr_4r_5Z^2)\sin(\phi+\theta_1)\cos\theta_5\dot{\theta}_5^2\\ &\quad + (m_Cr_4r_5 + J_mr_4r_5Z^2)\cos(\phi+\theta_1)\sin\theta_5\dot{\theta}_5^2 + B_mr_4^2Z^2\cos(\phi+\theta_1)\sin(\phi+\theta_1)\tan\theta_5\dot{\theta}_1\\ &\quad + \tfrac{1}{2}m_5r_4^2\cos^2(\phi+\theta_1)\tan\theta_5\dot{\theta}_1^2 + (m_cr_4^2 + J_mr_4^2Z^2)\cos^2(\phi+\theta_1)\tan\theta_5\dot{\theta}_1^2\\ &\quad - (\tfrac{1}{2}m_5r_4^2 + m_Cr_4^2 + J_mr_4^2Z^2)\sin^2(\phi+\theta_1)\tan\theta_5\dot{\theta}_1^2 + B_mr_4r_5Z^2\cos(\phi+\theta_1)\sin\theta_5\tan\theta_5\dot{\theta}_5\\ &\quad + \tfrac{1}{3}m_5r_4r_5\cos(\phi+\theta_1)\sec\theta_5\tan\theta_5\dot{\theta}_5^2 - \tfrac{1}{2}m_5r_4r_5\sin(\phi+\theta_1)\sin\theta_5\tan\theta_5\dot{\theta}_5^2\end{aligned}$$

$$
\begin{aligned}
&-(m_C r_4 r_5 + J_m r_4 r_5 Z^2)\sin(\phi+\theta_1)\sin\theta_5\tan\theta_5\dot{\theta}_5^2\\
&+(m_C r_4^2 + J_m r_4^2 Z^2)\cos(\phi+\theta_1)\sin(\phi+\theta_1)\tan^2\theta_5\dot{\theta}_1^2 + (m_C r_4 r_5 + J_m r_4 r_5 Z^2)\sin\theta_5\tan^2\theta_5\dot{\theta}_5^2\\
&+m_B(-4r_1^2\cos\theta_1\sin\theta_1\dot{\theta}_1^2)\\
&\equiv \hat{N}_1 + m_B\hat{N}_2, \qquad (A.2)
\end{aligned}
$$

$$
\hat{Q} = B^v - \mathbf{\Phi}_v^{\mathrm{T}}(\mathbf{\Phi}_u^{-1})^{\mathrm{T}}\mathbf{B}^u = K_t r_4 Z(\sin\theta_1 - \cos(\phi+\theta_1)\tan\theta_5), \qquad (A.3)
$$

$$
\begin{aligned}
\hat{D} &= D^v - \mathbf{\Phi}_v^{\mathrm{T}}(\mathbf{\Phi}_u^{-1})^{\mathrm{T}}\mathbf{D}^u\\
&= m_B(-\mu g r_1\sin(\theta_1+\phi) + \mu g r_1\cos\theta_1\tan\theta_2) + F_E(r_1\sin(\theta_1+\phi) - r_1\cos\theta_1\tan\theta_2)\\
&\equiv m_B\hat{D}_1 + F_E\hat{D}_2, \qquad (A.4)
\end{aligned}
$$

$$
\begin{aligned}
\dot{\hat{M}} = &-\tfrac{1}{3}m_5 r_4^2(-2\sec^2\theta_5\cos(\phi+\theta_1)\sin(\phi+\theta_1)\dot{\theta}_1 + 2\cos^2(\phi+\theta_1)\sec^3\theta_5\sin\theta_5\dot{\theta}_5)\\
&-4m_3 r_1^2\sin\theta_1\cos\theta_1\dot{\theta}_1 - (m_5 r_4^2 + m_C r_4^2 + J_m r_4^2 Z^2)2\sin(\phi+\theta_1)\cos(\phi+\theta_1)\dot{\theta}_1\\
&+(m_5 r_4^2 + 2m_C r_4^2 + 2J_m r_4^2 Z^2)\{-\sin^2(\phi+\theta_1)\tan\theta_5\dot{\theta}_1\sin(\phi+\theta_1)\tan\theta_5\\
&+\cos(\phi+\theta_1)[\cos(\phi+\theta_1)\tan\theta_5\dot{\theta}_1 + \sin(\phi+\theta_1)\sec^2\theta_5\dot{\theta}_5]\}\\
&-(m_C r_4^2 + J_m r_4^2 Z^2)\{2\cos(\phi+\theta_1)(-\sin(\phi+\theta_1))\tan^2\theta_5\dot{\theta}_1\\
&+2\cos^2(\phi+\theta_1)\tan\theta_5\sec^2\theta_5\dot{\theta}_5\} + m_B(-8r_1^2\sin\theta_1\cos\theta_1\dot{\theta}_1)\\
\equiv\ &\dot{\hat{M}}_1 + m_B\dot{\hat{M}}_2. \qquad (A.5)
\end{aligned}
$$

From Eqs. (23) and (24), we have the following functions:

$$
Y(\bullet) = \hat{Q}^{-1}\hat{M}_1(\lambda_e\dot{e} - \ddot{x}_B^*) - \hat{Q}^{-1}\hat{M}_1 2r_1\cos\theta_1\dot{\theta}_1^2 + \hat{Q}^{-1}\hat{N}_1 2r_1\sin\theta_1,
$$

$$
Z(\bullet) = \begin{bmatrix} \hat{Q}^{-1}(\lambda_e\dot{e} - \ddot{x}_B^*)\hat{M}_2 - \hat{Q}^{-1}\hat{M}_2 2r_1\cos\theta_1\dot{\theta}_1^2 + \hat{Q}^{-1}\hat{N}_2 2r_1\sin\theta_1 - \hat{Q}^{-1}\hat{D}_1 2r_1\sin\theta_1 \\ -\hat{Q}^{-1}\hat{D}_2 2r_1\sin\theta_1 \end{bmatrix}^{\mathrm{T}},
$$

$$
Y'(\bullet) = \hat{Q}^{-1}\hat{M}_1(\lambda_e\dot{e} - \ddot{x}_B^*) - \hat{Q}^{-1}\hat{M}_1 2r_1\cos\theta_1\dot{\theta}_1^2 + \hat{Q}^{-1}\hat{N}_1 2r_1\sin\theta_1 + \tfrac{1}{2}\dot{\hat{Q}}^{-1}\hat{M}_1 s + \tfrac{1}{2}\hat{Q}^{-1}\dot{\hat{M}}_1 s,
$$

$$
Z'(\bullet) = \begin{bmatrix} \hat{Q}^{-1}(\lambda_e\dot{e} - \ddot{x}_B^*)\hat{M}_2 - \hat{Q}^{-1}\hat{M}_2 2r_1\cos\theta_1\dot{\theta}_1^2 + \hat{Q}^{-1}\hat{N}_2 2r_1\sin\theta_1 - \hat{Q}^{-1}\hat{D}_1 2r_1\sin\theta_1 \\ +\tfrac{1}{2}\dot{\hat{Q}}^{-1}\hat{M}_2 s + \tfrac{1}{2}\hat{Q}^{-1}\dot{\hat{M}}_2 s \\ -\hat{Q}^{-1}\hat{D}_2 2r_1\sin\theta_1 \end{bmatrix}^{\mathrm{T}}.
$$

References

[1] F.J. Lin, R.F. Fung, Y.C. Wang, Sliding mode and fuzzy control of toggle mechanism using PM synchronous servomotor drive, *IEE Proceedings on Control Theory and Applications* 144 (1997) 393–402.

[2] R.J. Wai, C.H. Lin, F.J Lin, Adaptive fuzzy neural network control for motor-toggle servomechanism, *Mechatronics* 11 (2001) 95–117.

[3] R. J Wai, Robust fuzzy neural network control for nonlinear motor-toggle servomechanism, *Fuzzy Sets and Systems* 139 (2003) 185–208.

[4] F.J. Lin, R.J. Wai, Hybrid computed torque controlled motor-toggle servomechanism using fuzzy neural network uncertainty observer, *Neurocomputing* 48 (2002) 403–422.

[5] R.F. Fung, R.T. Yang, Motion control of an electrohydraulic actuated toggle mechanism, *Mechatronics* 11 (2001) 939–946.

[6] R.F. Fung, J.W. Wu, D.S. Chen, A variable structure control toggle mechanism driven by linear synchronous motor with joint Coulomb friction, *Journal of Sound and Vibration* 247 (2001) 741–753.
[7] Z.B. Li, Z.L. Wang, J.F. Li, A hybrid control scheme of adaptive and variable structure for flexible spacecraft, *Aerospace Science and Technology* 8 (2004) 423–430.
[8] L. Beji, Y. Bestaoui, Motion generation and adaptive control method of automated guided vehicles in road following, *IEEE Transactions on Intelligent Transportation Systems* 6 (1) (2005) 113–123.
[9] I. Petrovic, M. Brezak, Machine vision based control of the ball and beam, *Advanced Motion Control IEEE Seventh International Workshop* 3 (2002) 573–577.
[10] Y. Ju, S.K. Chang, B. Jong, S. Hong, M.H. Lee, F. Harashima, Vision based lateral control by yaw rate feedback, *The 27th Annual Conference of the IEEE Industrial Electronics Society C* (2001) 2135–2138.
[11] J.H. Park, Y.J. Lee, Robust visual servoing for motion control of the ball on a plate, *Mecatronics* 13 (2002) 723–738.
[12] O. Nasisi, R. Carelli, Adaptive servo visual robot control, *Robotics and Autonomous Systems* 43 (2003) 51–78.
[13] K. Astrom, B. Wittenmark, *Adaptive Control*, Addison-Wesley, Reading, MA, 1995.
[14] J.J.E. Slotine, W. Li, *Applied Nonlinear Control*, Prentice-Hall, Englewood Cliffs, NJ, 1991.
[15] J.J.E. Slotine, W. Li, Adaptive manipulator control: a case study, *IEEE Transactions and Automatic Control* 33 (1988) 995–1003.
[16] J.J.E. Slotine, W. Li, Composite adaptive control of robot manipulators, *Automatica* 25 (1989) 509–519.
[17] T.S. Lee, C.H. Lin, F.J. Lin, An adaptive H_∞ controller design for permanent magnet synchronous motor drives, *Control Engineering Practice* 13 (2005) 425–439.
[18] F.J. Lin, R.F. Fung, Y.S. Lin, Adaptive control of slider-crank mechanism motion: simulations and experiments, *International Journal of Systems Science* 28 (1997) 1227–1238.
[19] K.S. Narendra, A.M. Annaswamy, *Stable Adaptive System*, Prentice-Hall, Englewood Cliffs, NJ, 1988.